Porous carbon materials derived from olive kernels: application in adsorption of organic pollutants

Nadia El Ouahedy, Mohamed Zbair, Satu Ojala, Rachid Brahmi, Laurence Pirault-Roy

Porous carbon materials derived from olive kernels: application in adsorption of organic pollutants

Nadia El Ouahedy [1,2] • Mohamed Zbair [3] • Satu Ojala [3] • Rachid Brahmi [1] • Laurence Pirault-Roy [2]

[1] Laboratory of Coordination and Analytical Chemistry (LCCA), University Chouaïb Doukkali, El Jadida, Morocco

[2] Institut de Chimie des Milieux et Matériaux de Poitiers (IC2MP), Université de Poitiers UMR 7285 CNRS, 4, Rue M. Brunet, 86073 Poitiers Cedex 9, France

[3] Environmental and Chemical Engineering, Faculty of Technology, University of Oulu, Oulu, Finland

Corresponding author : Laurence Pirault-Roy laurence.pirault@univ-poitiers.fr

Abstract

Adsorption of organic pollutants (OPs), bisphenol A, and diuron, from aqueous solutions onto porous carbon materials (CMs) prepared from olive kernels, have been investigated. The effects of initial pH, initial OP concentration, temperature, and contact time on the adsorption capacity were studied. The adsorption of bisphenol A and diuron onto CMs was found to be optimal at pH 5.6 and 6.9, respectively. It was noticed that the adsorption of those organic pollutants from aqueous solution declined with increasing temperature and the process is exothermic. The rate of adsorption followed the second order kinetic equation. The equilibrium results showed that Langmuir model fits well with the data. The maximum adsorption capacities obtained using the best CM were 476 and 434 mg g^{-1} for BPA and diuron, respectively. The results showed that CMs made from olive kernels are an excellent and inexpensive biomass waste–derived sorbent.

Keywords: Porous carbon · Olive kernels · Adsorption · BPA · Diuron · Water treatment

1- Introduction

During the recent years, the Earth's ecosystem is being continuously contaminated by different pollutants, and their concentrations increase in aquatic systems. Some of them are persistent against the natural environmental degradation (chemical, biological, and photolytic reactions) (Lorenzo et al. 2018) and can cause significant harms to human health, animals, and the environment even at low exposure concentrations. Bisphenol A (BPA) and diuron were targeted as model pollutants. Those pollutants were chosen, on the one hand, according to human consumption and occurrence in the aquatic environment and, on the other hand, to their serious risk to human health, soil, and aquatic ecosystems as well as the environment. Moreover, they bioaccumulate and bio-magnify as their amounts shift up through the food chain.

Bisphenol A 4,4′-dihydroxy-2,2-diphenylpropane is a known endocrine disruptor (Bhatnagar et al. 2017). It is used in the manufacturing of polycarbonate plastics and epoxy resins, and it is found in a huge range of products including plastic containers for food and beverages, medical devices, sports equipment and thermal papers, and dental fillings and sealants (Acosta et al. 2018; Michałowicz 2014). Bisphenol A is an endocrine disruptor for human health officially recognized by the European

Chemicals Agency since 2017. Even at low levels of exposure to BPA, scientific studies report proven health effects in animals and suspected in humans. It is responsible for reproductive disorders and carcinogenic effects, especially on the animal mammary gland (Desbiolles 2016). Diuron (3-(3 4-dichlorophenyl)-1, 1-dimethylurea) is a type of phenyl urea herbicide that has been used for weed manage-ment in the pre- and post-germination stages (Liu et al. 2018). It degrades slowly in water bodies or in the environment, and it is toxic for both flora and fauna especially in aquatic eco-systems (Liu et al. 2018; Giacomazzi and Cochet 2004). In humans, Diuron can cause kidney disease, hemolytic anemia, compensatory hematopoiesis, and endocrine problems, and it is also potentially carcinogenic.

Great efforts have been devoted for developing different ways to remove organic contaminants from the aquatic environment. These methods include for example adsorption (Zbair et al. 2018a, b, c, d), electrochemical treatment (Rice et al. 2018), photocatalytic degradation (Tolosana-Moranchel et al. 2019), and membrane filtration (Fu and Zhang 2018). Among these, adsorption is considered as a low cost-effective and efficient one. In particular, the adsorption on activated car- bon (AC) is one of the most effective and widely used methods for purifying water. Many different raw materials have been used for production of activated carbon, including biomass waste such as slash pine impregnated by $ZnCl_2$. The adsorbent prepared has a specific surface area of 1185 $m^2\ g^{-1}$ and an excellent CO2 adsorption capacity (4.22–5.44 mmol m^{-2}) (Boshir et al. 2019). Brown coal was also tested with Fe_3O_4 as a bi-functional additive to prepare a magnetic activated carbon (Jiang et al. 2019) with a specific surface area of 525 $m^2\ g^{-1}$. Petrochemical resins physically activated by CO_2 to prepare activated carbon with a high specific surface area about 1410 $m^2\ g^{-1}$ were also used for supercapacitor electrode applications (Lee et al. 2019). Other studies investigated also the use of industrial waste materials such as industrial sisal fibers via chemical activation by H_3PO_4 to produce activated carbon with a high specific surface area about 1296 $m^2\ g^{-1}$ (Dizbay-Onat et al. 2017). From the available raw materials, biomaterials and especially the biowaste materials should be favored, since they are sustainable and environmentally sound alternative to coal and petrochemical resins. For example, Spain, the world's largest producer of olive oil, produces 37,500 tons of olive kernels waste every year. This waste is currently used to produce ethanol via fermentation or energy due to its good calorific value. An alternative route for current use could be the transformation of olive kernels to porous carbon-based adsorbent for environ- mental remediation. The application of ACs prepared from olive kernels in wastewater treatment has been reported for the ad- sorption of dye (Hazzaa and Hussein 2015). First, the olive kernels were carbonized at 800 °C for 60 min, then the prepared materials were tested to adsorb methylene blue dye but the authors did not mention the specific surface area of the obtained activated carbon. It resulted in 16 mg g^{-1} maximum adsorption capacity at 25 °C. The removal of heavy metals was also discussed (Alslaibi et al. 2013). In this work, the olive kernels were activated chemically and microwaved with KOH at a frequency of 2.45 GHz and power level of 264 W. The sample obtained with a 790 $m^2\ g^{-1}$ surface area was then tested to adsorb cadmium (Cd^{2+}). A maximum adsorption capacity of 12 mg g^{-1} was evidenced. These results indicated that such activated carbon can be used successfully as a low-cost adsorbent in several applications.

In-depth studies have been performed on the adsorption of BPA on activated carbon. Supong et al investigated BPA adsorption on activated carbon prepared from Tithonia diversifolia biomass chemically and thermally activated by potassium hydroxide and using a pyrolysis temperature of 700 °C. The authors evidenced that the best prepared activated carbon exhibited a 854 $m^2\ g^{-1}$ surface area and reached a 98% maximum removal for 0.2 g adsorbent dose and 40 mg L^{-1} initial concentration of BPA. They also suggested that the adsorption of BPA onto the activated carbon was mainly due to the adsorbent–adsorbate interactions where it proceeded via chemisorption (Supong et al. 2019).

Tchikuala et al studied the adsorption of diuron using activated carbon prepared from wood waste

by physical activation using carbon dioxide at 800 °C. As a result, they found that the material prepared has high specific surface area 1214 m^2 g^{-1} and its maximum adsorption capacity of diuron reached 400 mg g^{-1} .The batch adsorption results indicated that the influential factors in the uptake of diuron were the structural characteristics of the activated carbon, namely the pore volume and the specific surface area complemented by their chemical nature, i.e., the basic nature of the materials prepared favored the diuron adsorption (Tchikuala et al. 2017).

With this background, the aim of the current work was, in the first place, the preparation of porous carbon materials (CMs) from olive kernels using phosphoric acid. During preparation steps, the activation temperature (600 °C and 700 °C) and the impregnation ratio (1:4, 1:1) were varied in order to determine their effects on the porous structure of the CMs. The second objective of this study was to evaluate performance of all prepared CMs in the adsorption of BPA and diuron. The physicochemical characteristics of the pre- pared adsorbents and the surface morphology were determined in order to explain the adsorption performance obtain- ed. Then, the influence of the main adsorption parameters such as pH and temperature was analyzed, and finally the adsorption kinetics, equilibrium isotherms, and thermodynamic parameters were determined. All the graphics in this work were created using Excel 2013 and Origin 9.0 program.

2- Experimental

2.1 Preparation of porous carbon

In the beginning of CM preparation, olive kernels were thoroughly washed with distilled water and dried in an oven at 120 °C for 12 h. Then, they were crushed and sieved to obtain a powder of defined size (< 160 μm). This micrometric powder ensures the access of the activating agent to the interior of the raw material (olive kernels) and thus increases the contact surface allowing to optimize interactions. The chemical activation method was done by using phosphoric acid H_3PO_4 as an activating agent. The chemical activation consists of three steps. The first step is the impregnation of the olive kernels in aqueous solutions of the phosphoric acid. Impregnation was performed with two different mass ratios (raw material : activating agent) (1:4) and (1:1). Those ratios were chosen because they are the most efficient ratios used for the activation by H_3PO_4 according the literature in terms of prepared material yield, specific surface area, and adsorption capacity (Yorgun and Yıldız 2015; Kiliç et al. 2012; Kumar and Jena 2016). The second step is the pyrolysis of the impregnated olive kernels under N_2 with a flow rate of 10 mL min^{-1} for 2 h. Pyrolysis was carried out at two different temperatures 600 °C and 700 °C targeted from the thermal decomposition results of olive kernels discussed later in the "TGA-DTA analysis" section.

Thirdly, the product was washed with solution of 10%wt HCl at elevated temperature (60 °C, 6 h) to remove partially the mineral impurities. Then, CMs were washed with distilled water and dried at 120 °C. In the end of the preparation, the activated carbon obtained has been ground and sieved to have a unified particle size (< 0.35 μm). Table 1 summarizes the operating conditions used for each sample.

Table 1. Summary of the operating conditions used during the preparation for each carbon material and their coding.

	Mass ratio (Raw material: Activating agent)	Temperature (°C)	Code
Phosphoric Acid (PA)	1:1	700	**CM11-700**
	1:1	600	**CM11-600**
	1:4	700	**CM14-700**
	1:4	600	**CM14-600**

2.2 Characterization

The porous structure of the CMs was characterized by N_2 adsorption/desorption at 77 K using the Micromeritics- ASAP 2020 apparatus. The morphology of olive kernels and CMs was characterized by field emission scanning electron microscope (ZEISS ULTRA Plus). The content of carbon, hydrogen, and nitrogen was determined by elemental analysis using NA2100 Protein analyzer from Thermoquest. The sur- face charge of carbon materials was determined using Zetasizer Nano series of Malvern device. The thermal proper- ties of olive kernels were investigated by thermogravimetric analysis (TGA) using a SDT Q600 TA Instruments analyzer.

2.3 Adsorption experiments

Adsorption experiments were carried out using 200 mL pollutant solution (20 mg L^{-1} and 35 mg L^{-1} of BPA and diuron, respectively) and a weighed amount of CMs (10 mg). The flasks containing pollutant solution and adsorbent were agitated at constant speed (300 rpm) at selected constant temperatures (20, 40, 60 °C). The effect of the contact time was studied by varying the adsorption time from 0 to 180 min at 25 °C. At the end of the adsorption period, the solution was separated using 0.2-µm milli-pore syringe filters. The pollutant concentrations were measured by a UV spectrophotometer at 277 nm for bisphenol A and at 248 nm for diuron. The effect of the contact time was studied by varying the adsorption time from 0 to 180 min at 25 °C. The effect of initial pH of the pollutant solution was studied over a range from 2 to 11. The pH values of the solutions were adjusted using 0.1 M HCl and 0.1 M NaOH solutions. To study the effect of initial con- centration, the experiments were performed at various concentrations ranging from 10 to 100 mg L^{-1} for BPA and 5 to 35 mg L^{-1} for diuron.

The calculation of the removal efficiency and adsorption capacity as well as kinetic, equilibrium, and thermodynamic parameters of BPA and diuron adsorption onto CMs are presented in Table 2.

Table 2. Mathematical equations and models using in this work

Mathematical Equations		Parameter descriptions	References
Adsorption capacity	$Q_{e,t} = \frac{(C_0 - C_{e,t}) \times V}{m}$	C_0 (mg . L^{-1}) and $C_{e,t}$ (mg . L^{-1}): initial and equilibrium concentrations, respectively. m (g): weight of adsorbent. V (L): volume of BPA and Diuron.	(Wang et al. 1998)
Removal efficiency	$R(\%) = \left(\frac{C_0 - C_{e,t}}{C_0}\right) \times 100$		(Garg et al., 2003)
Kinetic models			
Pseudo-first order	$Q_t = Q_e(1 - \exp^{-K_1 t})$	Q_e and Q_t (mg . g^{-1}): adsorbed BPA and Diuron amounts at equilibrium and at times t, respectively. K_1: rate constant; $K_{2:}$ rate constant	(Nathan and Scobell, 2012)
Pseudo-second order	$Q_t = \frac{(K_2 Q_e^2 t)}{(1 + K_2 Q_e t)}$		(Ho and McKay, 1999)
Isotherm models			
Langmuir isotherm	$Q_e = \frac{Q_m K_L C_e}{1 + K_L C_e}$	K_L: direct measurement of the intensity of the adsorption process; Q_m: maximum adsorption capacity.	(Langmuir, 1916)
Freundlich isotherm	$Q_e = K_F C_e^{\frac{1}{n}}$	$K_{F:}$ adsorption capacity; n: intensity of adsorption; 1/n=0 irreversible; 1/n>1 unfavorable 0<1/n<1 favorable.	(Freundlich, 1907)
Thermodynamic equations			
Gibbs free energy	$\Delta G^{\circ} = -RT \ln K_d$	ΔG°: Gibbs free energy change; K_d: equilibrium constant; R: gas constant; T: temperature.	(Tran et al. 2017; Tsai et al 1995)
Van't Hoff equation	$\ln K_d = \frac{\Delta S^{\circ}}{R} - \frac{\Delta H^{\circ}}{RT}$	ΔS°: Entropy variation; ΔH°: Enthalpy variation.	(Tran et al., 2017)

3- Results and discussion

3.1 Characterization of porous carbon

3.1.1 Elemental analysis

Table 3 summarizes the elemental analysis results of olive kernels and the prepared CMs. The elemental analysis of the raw material (olive kernels) showed a high carbon content, which favors its use for

porous carbon materials synthesis. Essentially, olive kernel is a lignocellulosic material, with hemicellulose, cellulose, and lignin as the main compounds. The chemical activation or pyrolysis process involves a large number of reactions, where these polymeric structures decompose and form solid product (coal), liquids (called as tars), and gases (volatiles compounds). The gaseous and liquid products removed are mainly composed of the non- carbon elements of the raw material, like hydrogen, oxygen, and nitrogen (García et al. 2014).

Table 3 evidenced that with increasing pyrolysis temperature from 600 to 700 °C, the carbon and hydrogen contents of the activated carbon samples decreased. When the concentration of phosphoric acid (impregnation ratio) increase from 1 to 4, the content of hydrogen decreased as well as the content of nitrogen. The significant reduction in H and O contents was due to the major dehydration reaction (removal of hydroxyl groups) of the hemicellulose, cellulose, and lignin during activation and pyrolysis which led to the increase of the relative proportion of the element C (Wang et al. 2020). The content of S decreased clearly after the preparation process resulting from the volatilization of H2S and SOx. Furthermore, the denitrification of the different CMs can be explained by the loss of the nitrogenous compounds with volatile matters (Xing et al. 2019).

The O/C molar ratio has been used as a reference for surface hydrophilicity, because it reveals the content of polar groups resulting mainly from carbohydrates. In Table 3, the results show that the CM samples (i.e., CM11-700, CM14-600, CM14-700, and CM11-600) had approximately similar O/C molar ratios, signifying that they shared similar affinity for water. Additionally, the H/C molar ratio indicates the degree of aromatization and carbonization (Tran et al. 2018).

The H/C molar ratio of all the prepared samples decreased remarkably compared with the raw material implying that the CMs have higher aromatic content and they are thermally more stable.

Table 3. Elemental analysis of CMs

	N (wt%)	C (wt%)	H (wt%)	S (wt%)	O [a] (wt%)	H/C [b] (wt%)	O/C [b] (%)
Olive kernels	0.5	45.5	6.0	0.2	47.7	1.6	0.8
CM11-700	0.3	69.8	1.3	0.0	28.5	0.2	0.3
CM11-600	0.3	75.0	1.6	0.0	23.1	0.2	0.2
CM14-700	0.2	70.9	0.9	0.0	27.9	0.1	0.3
CM14-600	<0.1	72.2	1.3	0.0	26.4	0.2	0.3

[a] **Calculated by difference.**
[b] **Atomic ratio.**

3.1.2 TGA-DTA analysis

To target the optimal temperature for the pyrolysis step, the thermal stability of olive kernel powder was evaluated by thermal analysis (TGA-DTA) between 25 and 900 °C under inert conditions (Ar; purity ≥ 99.5%). The results (Fig. 1) showed that the thermal decomposition of olive kernels exhibited a total mass loss of 68.97%, suggesting that the com- position of olive kernels is quite comparable with other similar ligno-cellulosic biomass. The first endothermic peak observed between 25 and 150 °C is assigned to dehydration reactions. The second and third exothermic peaks around 267 °C and 329 °C are related to the major weight loss, and can be attributed to the decomposition of hemicelluloses (150–270 °C) and celluloses (270–450 °C) via the formation of volatile com- pounds, essentially short-chain aliphatic hydrocarbons (García et al. 2014; Som et al. 2009). Lignin is thermally more stable and its degradation happens slowly under a wide temperature range from 100 to 900 °C (Özveren and Özdoğan 2013). The

small endothermic peak located between 650 and 750 °C corresponds to the carbonate's thermal degradation. Above 550 °C, the weight loss was low indicating that the basic structure of the material has been formed. Based on these results, the selected pyrolysis temperatures were 600 °C and 700 °C to guarantee the production of the thermallystable porous carbon materials.

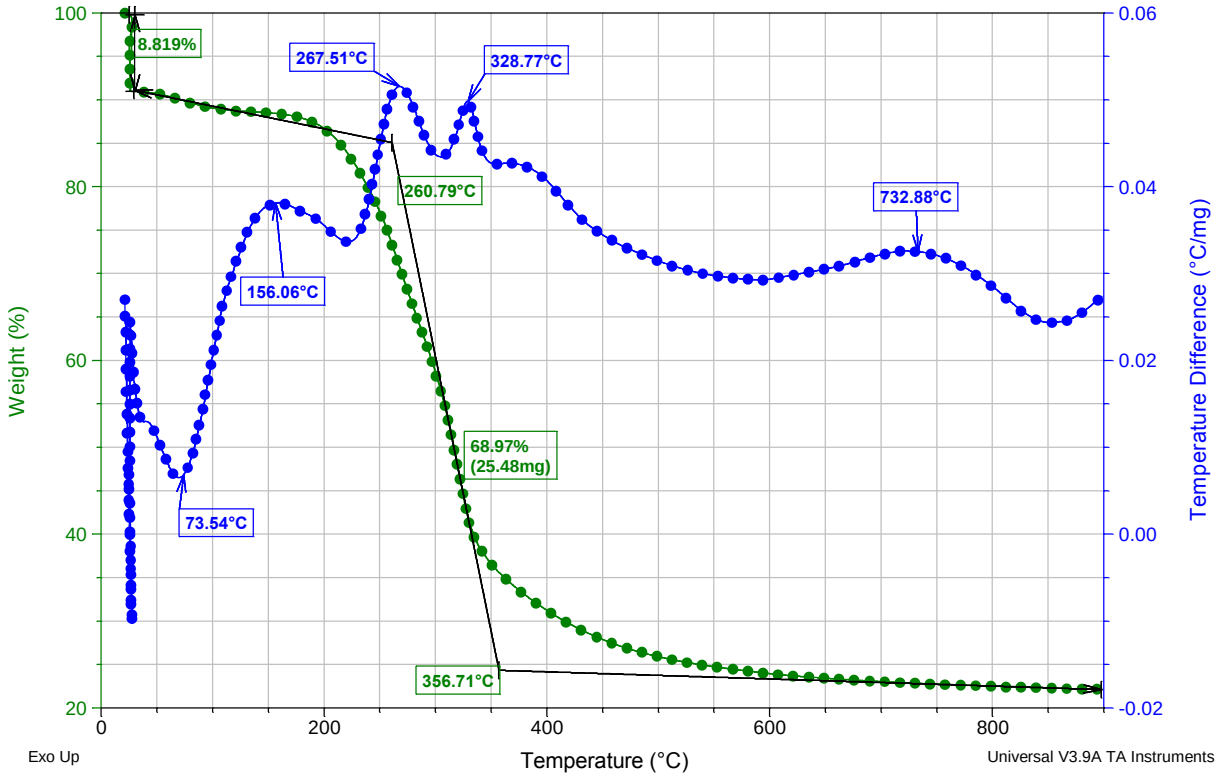

Fig 1. Thermal analysis (TGA-DTA) of olive kernels under argon atmosphere

3.1.3 N_2-Physisorption results

The prepared materials were analyzed by nitrogen physisorption in order to check the improvements of their textural properties. The adsorbents CM11-700 and CM11- 600 exhibited (Fig. 2) the type I isotherms (Langmuir isotherm) according to IUPAC classification. However, CM14-600 and CM14-700 displayed a type IV isotherm, demonstrating the presence of a mesoporous structure. The hysteresis loops of the isotherms of CM14-600 and CM14-700 samplesare H2b type corresponding to cage-like mesopores (Thommes et al. 2015; Bolivar et al. 2017). Table 4 presents the specific surface area, total pore volume, and average pores size of the CM samples. All samples exhibit a high specific surface area (higher than 1100 $m^2\ g^{-1}$), which is promising for adsorption applications. The highest specific surface area (1472 $m^2\ g^{-1}$) was obtained for CM11-700.

The effect of pyrolysis temperature and mass ratio of the preparation of CMs on S_{BET} is shown in Fig. 3. To have the highest surface area S_{BET}, it is necessary either to set the concentration of H_3PO_4 low and pyrolysis temperature high (mass ratio (1:1) and 700 °C) or to set the concentration of H_3PO_4 high and pyrolysis temperature low (mass ratio (1:4) and 600 °C) (Fig. 3). This observation means that a compromise between the mass ratio and temperature should be deter- mined as it seems that these two parameters are interdependent. No significant modification of the pore diameter is evidenced by changing the temperature of pyrolysis and the mass ratio.

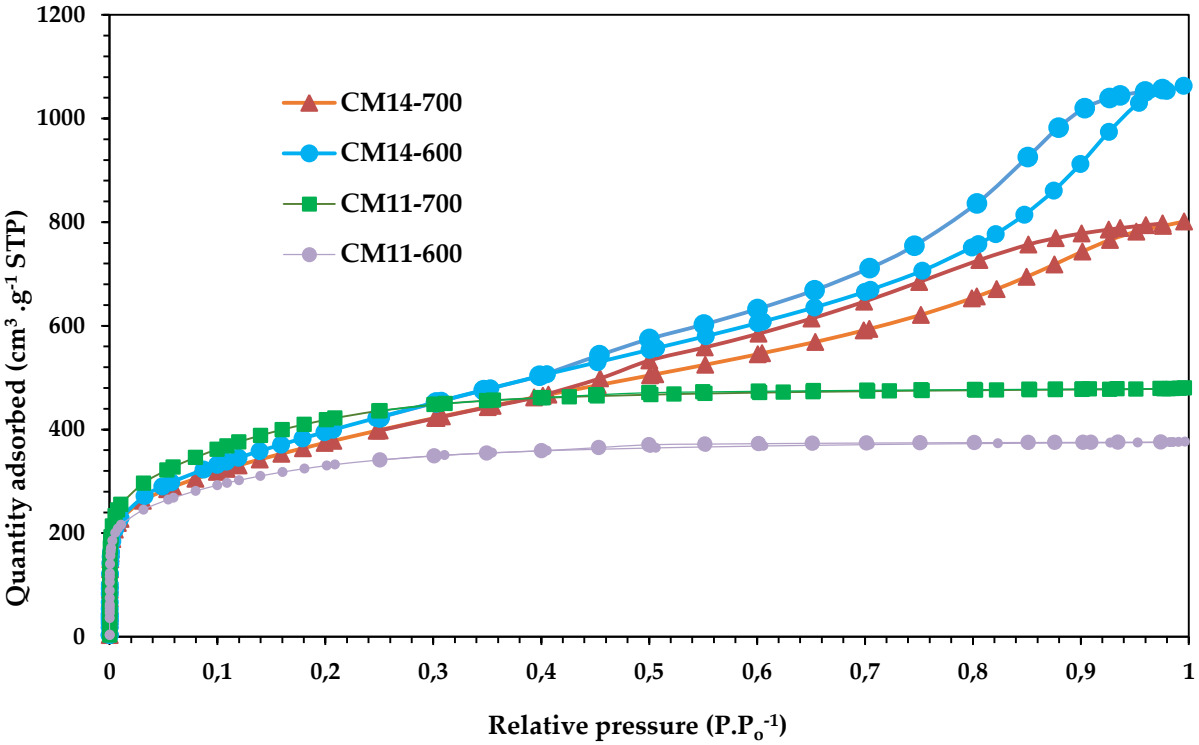

Fig 2. Adsorption-desorption isotherms of N_2 on CMs

Table 4. Textural properties of the activated carbons prepared

	S_{BET} ($m^2 . g^{-1}$)	Total pore volume ($cm^3 . g^{-1}$)	Average pores size-BJH (nm)
CM11-700	1472	0.50	1.1
CM11-600	1141	0.41	1.1
CM14-700	1341	0.44	1.2
CM14-600	1431	0.45	1.2

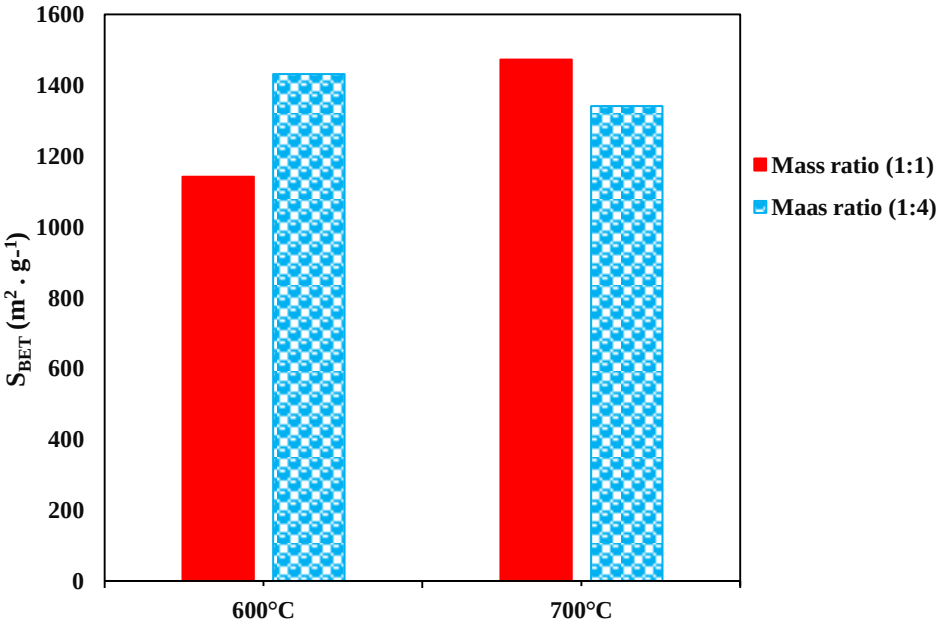

Fig 3. Evolution of CM's surface area according pyrolysis temperature and mass ratio of H_3PO_4 used to transform olive kernels

3.1.4 Scanning electron microscopy results

Scanning electron microscopy (SEM) was used to study the surface morphology of the raw material (olive kernels) and the prepared CMs. The results presented in Fig. 4 evidenced noticeable differences in the morphology of the samples. Firstly, the structure of the olive kernels is dense and almost non-porous, but after the chemical activation by H_3PO_4 followed by a pyrolysis, a remarkable degradation of the microstructure due to the decomposition of organic matter during the preparation is observed creating a porous surface. The cavities visible on the surface of CMs are created by the evaporation of the activating agent. On the other hand, discussing the effect of the mass ratio and pyrolysis temperature on the morphology of the materials prepared, it is evident from the images that:

- For the CM11-700 and CM11-600, the increase of the pyrolysis temperature favors the micropore development, which agrees well with the N_2 adsorption and desorption results. These changes of morphology are associated with the loss and the volatilization of the organic compounds of the raw material which created the voids and pores within its matrix (Hazzaa and Hussein 2015).
- Significant differences in the morphological features of the mass ratio (1:4) CMs compared with (1:1) mass ratio samples can be observed, which are confirmed by N2 ad- sorption and desorption results. According to the isotherms obtained, the mass ratio (1:4) develops isotherms type IV which are attributed to the mesoporous structure according to IUPAC classification. The development of this mesoporosity when the amount of H_3PO_4 increased is mainly due to the cell dilation between the various biopolymers that compose the olive kernel, caused by phosphate and polyphosphate bridges (Nieto-Delgado and Rangel-Mendez 2011).

In addition, the porosity generated in the materials after activation as observed by SEM analysis will allow the diffusion of BPA and diuron through the CMs.

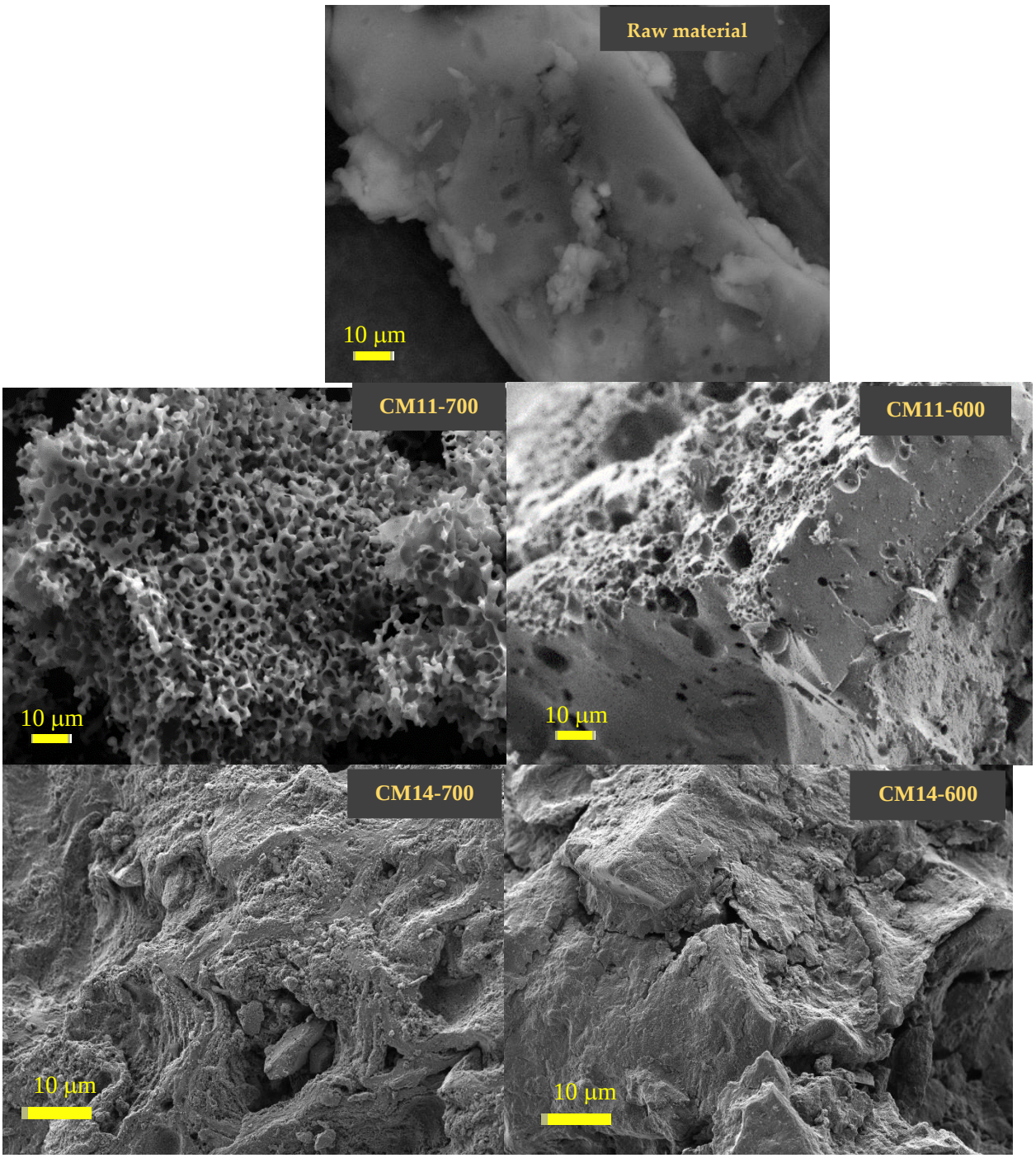

Fig 4. SEM images of raw materials and activated materials.

Effect of pH on the adsorption

The pH value of the solution is one of the most critical param- eters to control the adsorption process. It can be noted from Fig. 5a, that when pH was less than 5.6, the BPA adsorption on CMs prepared at 700 °C remains nearly constant while for those prepared at 600 °C, their adsorption capacities increase. However, when the pH was higher than 5.6, the adsorption decreased considerably for all the CMs. The diuron adsorption onto CMs was behaving differently, and adsorption was increased as the pH increased (Fig. 5b). These changes in the BPA and diuron adsorption onto CMs are related to the charge of BPA and diuron species and the sur- face charge of CMs that depends on the pH of the solution. For pH less than 8.0, BPA molecules are undissociated, while an anionic species, BPA^{-}, appears at pH higher than 8.0 values owing to deprotonation constant of BPA (pKa = 9.8). Additional anionic species, BPA^{2-}, can exist at pH values between 9.0 and 12.0, due to second deprotonation (pKa = 10.3) (López- Ramón et al. 2019). Moreover, the zeta potential measurements (Fig. 5c) showed that all the CMs are negatively charged whatever the pH. Thus, when the pH increased leading to BPA^{-} or BPA^{2-} species formation, electrostatic repulsion between these anions and CMs occurred which explains the decrease in BPA removal efficiency. For diuron (D), the pKa value is estimated to be 3.7 (Yang et al. 2008; Deng et al. 2012) expecting that the cationic species (DH^{+}) strongly predominated at pH below 1.7, whereas the neutral one (D) was the main species at pH higher than 5.7 (Fontecha-Cámara et al. 2007; Zbair et al. 2018a, b, c, d). Consequently, at lower pH, electrostatic attraction happens between negatively charged CMs (Fig. 5c) and the cationic diuron molecules. However, at pH higher than 5.7, the diuron molecule is neutral and the CMs are negatively charged; henceforth, non-electrostatic interactions are predominated. The results presented in Fig. 5b evidenced that such neutral diuron species is adsorbed on CMs, and that their quantity increased when pH in- creased. Previous studies performed by Fontecha-Cámara (Fontecha-Cámara et al. 2008) suggested that the solubility of diuron decreased with the presence of other ions and led to an increase in the adsorption capacity due to an increase in hydrophobic interactions.

Thus, the adsorption can remain at relatively high level. To summarize the results, BPA adsorption is favorable under acidic conditions, whereas diuron adsorption is favorable under basic ones. These outcomes are in accordance with the previous research on BPA and diuron adsorption onto carbon materials (Bautista-Toledo et al. 2005; Tsai et al 2006; Zbair et al. 2018a, b, c, d). Later adsorption experiments of this study were carried out at the pH of solution without adjustment.

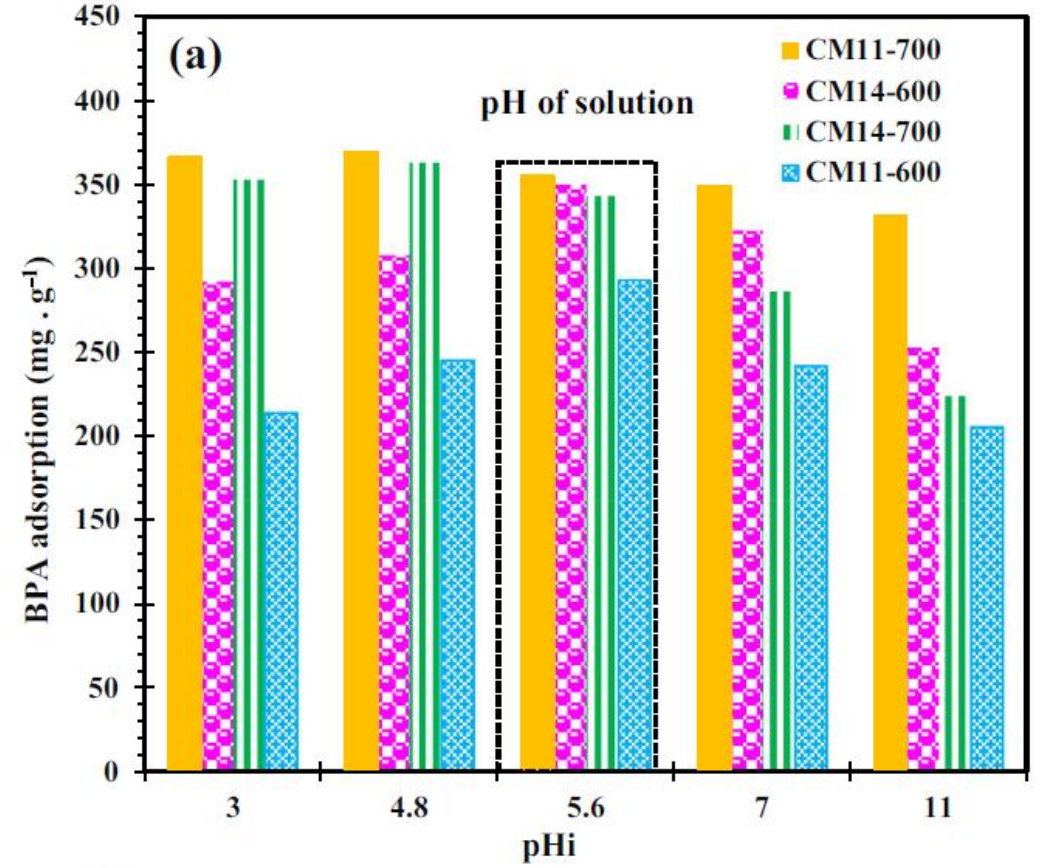
(a)
pH of solution
CM11-700
CM14-600
CM14-700
CM11-600
BPA adsorption (mg . g-1)
450
400
350
300
250
200
150
100
50
0
3
4.8
5.6
7
11
pHi

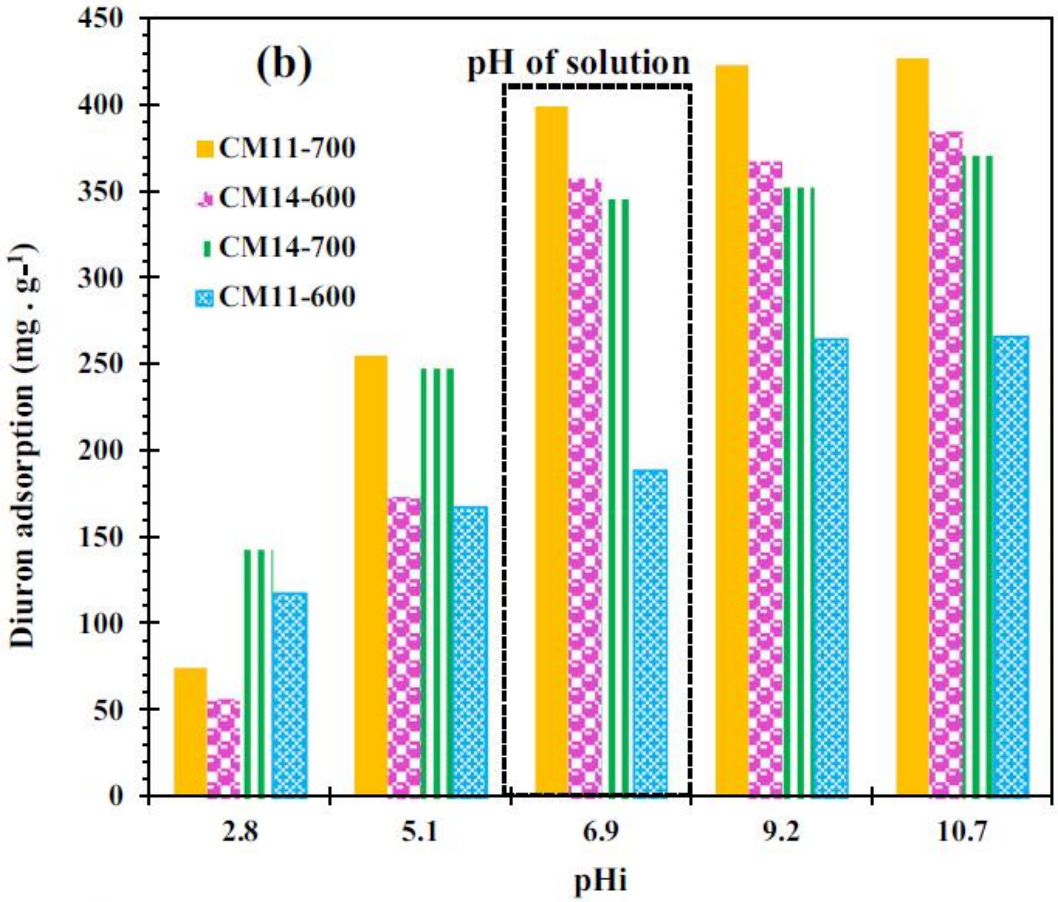
(b)
pH of solution
CM11-700
CM14-600
CM14-700
CM11-600
Diuron adsorption (mg . g-1)
450
400
350
300
250
200
150
100
50
0
2.8
5.1
6.9
9.2
10.7
pHi

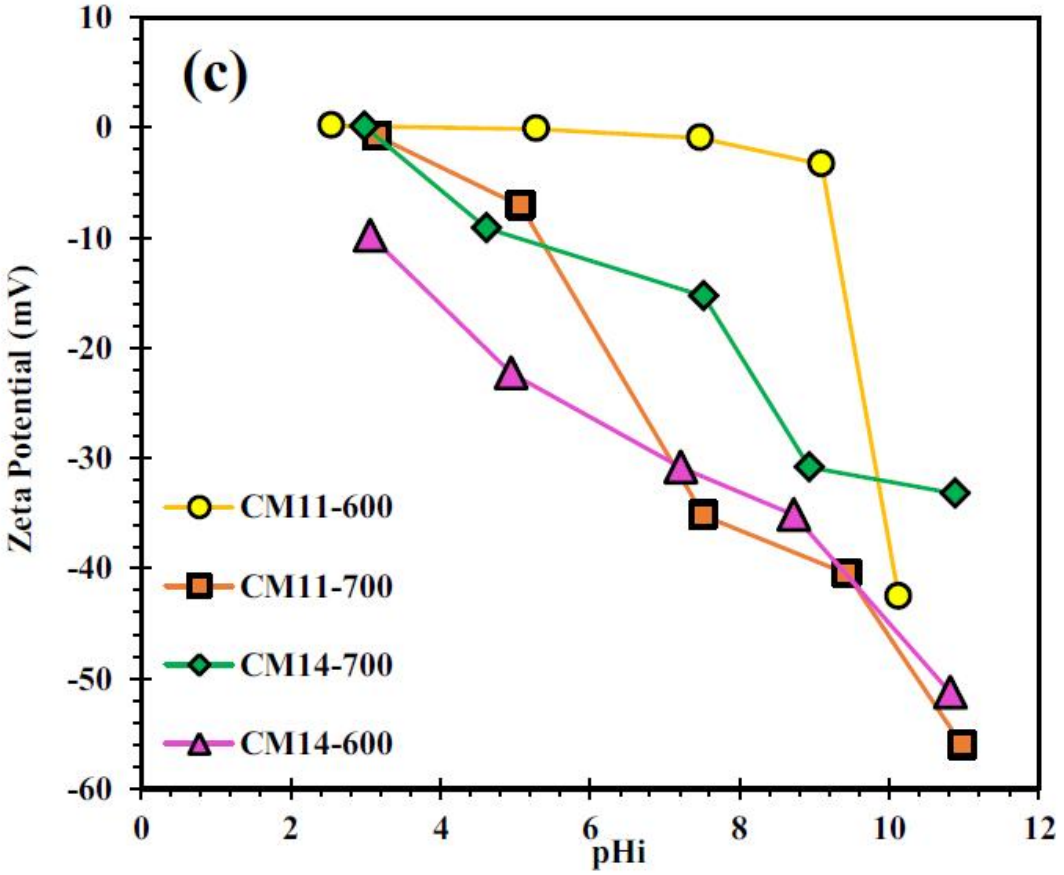

Fig 5. Effect of pH on (a) BPA adsorption, (b) Diuron adsorption and (c) Zeta potential of all CMs.

3.3 Kinetic study

The kinetics of adsorption of BPA and diuron onto CMs was examined using nonlinear pseudo-first order (P-1st-O) and pseudo-second order (P-2nd-O) kinetic models. The kinetic plots and appropriate parameters of the models are displayed in Figs. 6 and 7 and Table 5. Concerning adsorption kinetics of BPA (Fig. 6 and Table 5), the SD values of P-1st-O kinetic model vary from 7 to 20 while those of P-2nd-O model vary from 2 to 7. Moreover, the R^2 of P-1st-O are ranged between 0.608 and 0.894, whereas R^2 of P-2nd-O vary from 0.997 to 0.999. Thus, the P-2nd-O model has the lowest standard deviation (SD) with the experimental values and thus the highest R^2 values. In the case of diuron kinetics of adsorption (Fig. 7 and Table 5), the SD values of P-1st-O kinetic model fluctuate from 2 to 4, while those of P-2nd-O model vary from 2 to 3. Likewise, the R^2 of P-1st-O are extended between 0.677 and 0.943, whereas R^2 of P-2nd-O vary from 0.993 to 0.999. Consequently, the P-2nd-O model describes better the adsorption kinetics of BPA and diuron onto CMs. This conclusion was also proposed for the removal of BPA on activated carbon prepared by steam activation and hydrochar (Zbair et al. 2018a, b, c, d).

The parameter $t_{0.5}$, which is the time required to reach 50% of the equilibrium value obtained for BPA and diuron adsorption, was calculated by interpolation from the fitted P-2nd-O kinetic curve. The $t_{0.95}$ values were determined similarly. It was observed that $t_{0.5}$ is about between 9 and 15 min for BPA and lower than 1 min for diuron onto all CMs. The maximum of $t_{0.95}$ observed is about 68 min and 16 min for BPA and diuron, respectively (Table 5). For further tests, the BPA and diuron contact time of

adsorption onto CMs was fixed at 120 min to ensure reaching the equilibrium.

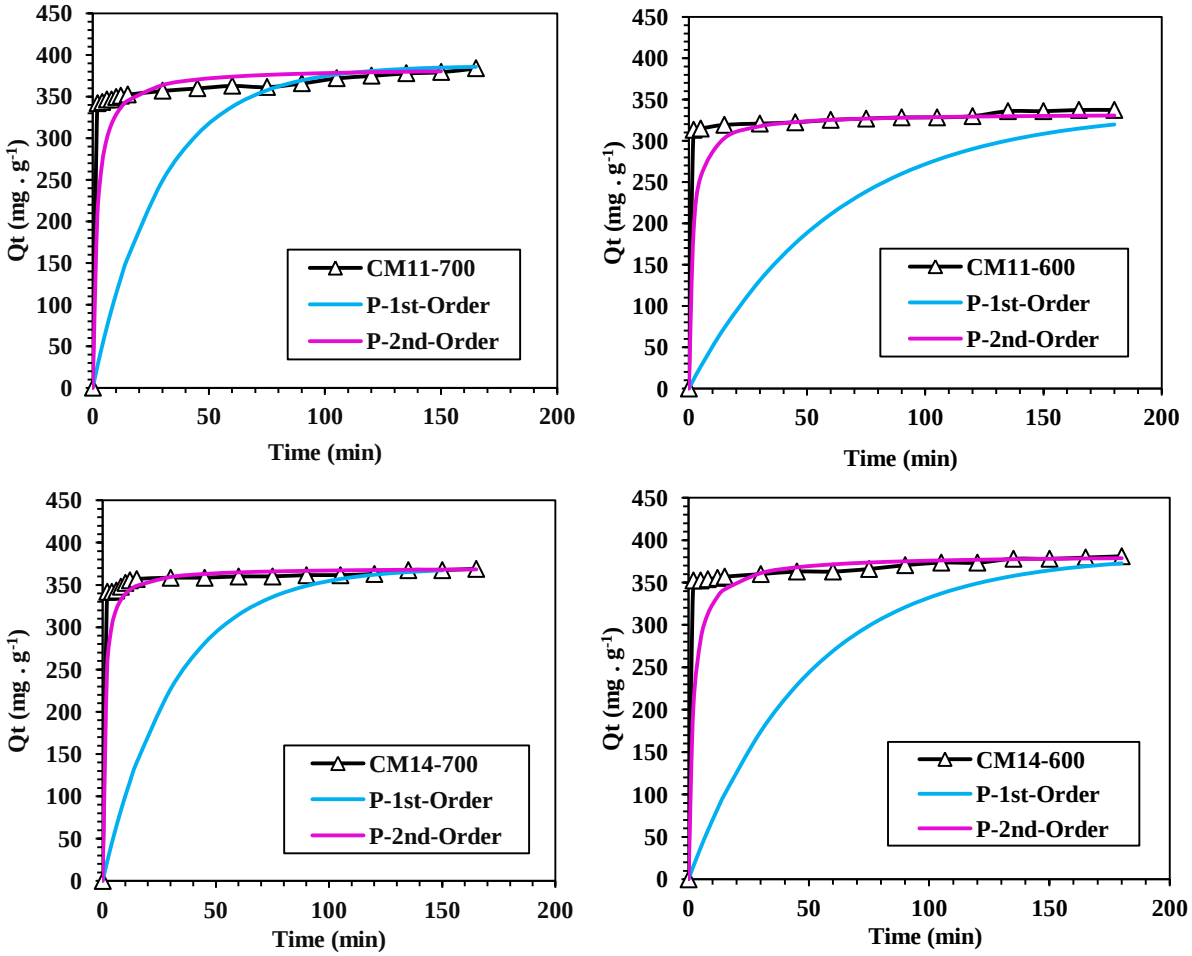

Fig 6. Adsorption kinetics of BPA onto porous carbon materials.

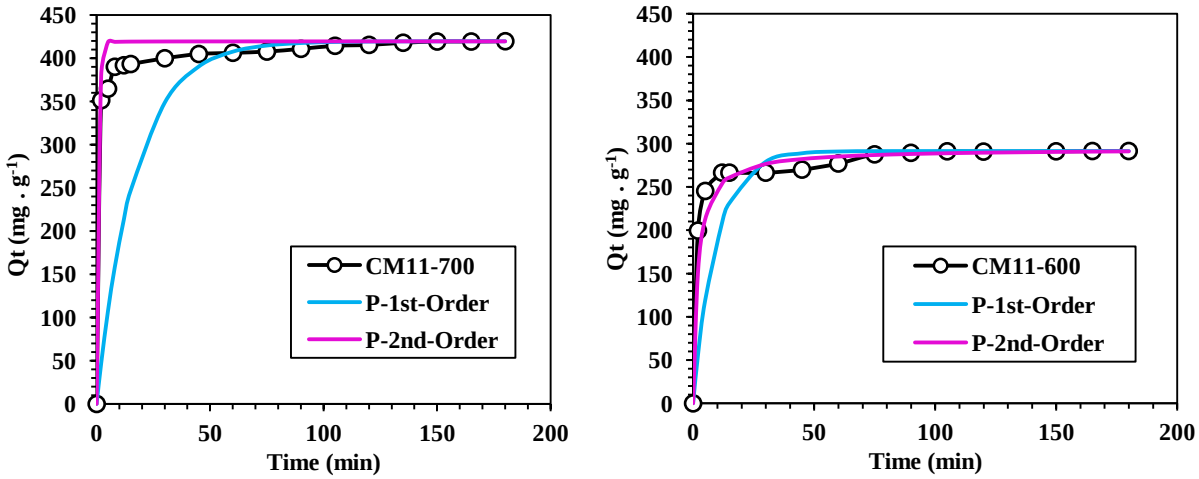

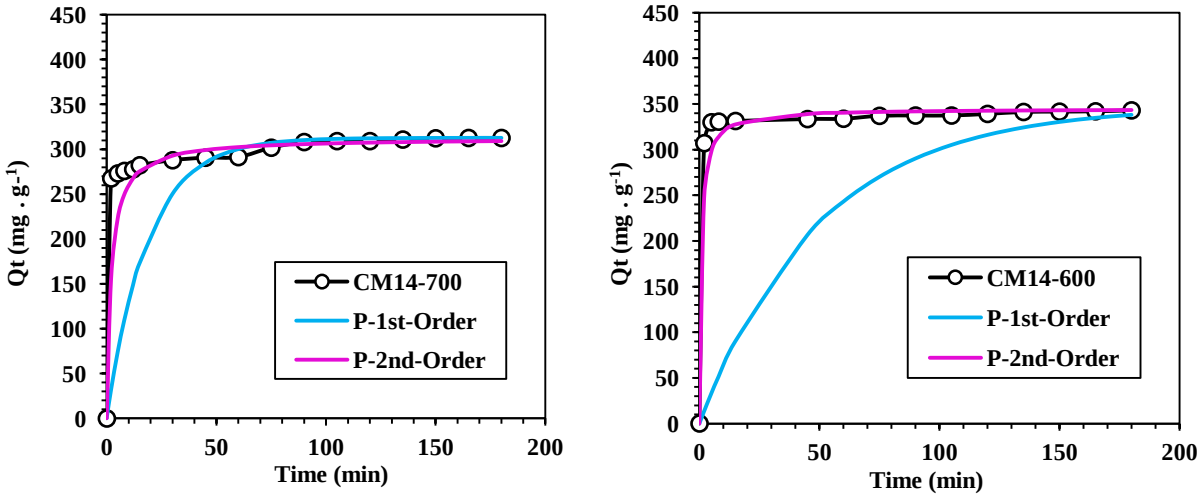

Fig 7. Adsorption kinetics of Diuron onto porous carbon materials.

Table 5. Kinetic and equilibrium adsorption parameters.

	CM11-700	CM14-600	CM14-700	CM11-600
Bisphenol A				
Pseudo-First Order				
Qe,cal (mg . g^{-1})	354	378	332	319
K_1 (min^{-1})	$3.4 . 10^{-2}$	$1.5 . 10^{-2}$	$3.1 . 10^{-2}$	$1.6 . 10^{-2}$
R^2	0.894	0.768	0.879	0.608
SD (mg . g^{-1})	20	13	7	7
Pseudo-Second Order				
Qe,cal (mg . g^{-1})	384	380	368	330
K_2 (g. mg^{-1}. min^{-1})	$1.4 . 10^{-3}$	$1.4 . 10^{-3}$	$2.9 . 10^{-3}$	$2.0 . 10^{-3}$
R^2	0.999	0.998	0.997	0.999
SD (mg . g^{-1})	6	2	2	7
$t_{0.5}$ (min)	14.0	15.0	9.0	9.0
$t_{0.95}$ (min)	66.0	68.0	31.0	36.0
Diuron				
Pseudo-First Order				
Qe,cal (mg . g^{-1})	418	352	295	282
K_1 (min^{-1})	$9.9 . 10^{-2}$	$7.2 . 10^{-2}$	$8.9 . 10^{-2}$	$9.6 . 10^{-2}$
R^2	0.943	0.677	0.906	0.932
SD (mg . g^{-1})	3	2	4	3
Pseudo-Second Order				
Qe,cal (mg . g^{-1})	410	340	301	294
K_2 (g. mg^{-1}. min^{-1})	$6.0 . 10^{-3}$	$1.3 . 10^{-3}$	$9.0 . 10^{-3}$	$3.0 . 10^{-3}$
R^2	0.993	0.997	0.999	0.999
SD (mg . g^{-1})	2	2	3	2
$t_{0.5}$ (min)	0.5	0.1	0.7	0.8
$t_{0.95}$ (min)	7.0	4.0	7.0	16.0

3.4 Equilibrium studies

Adsorptions isotherms of BPA and diuron were deter- mined by using BPA (10–100 mg L^{-1}) and diuron (5–35 mg L^{-1}) solutions and samples CM11-700, CM14- 600, CM14-700, and CM11-600. The Langmuir and Freundlich plots of BPA and diuron were drawn (Figs. 8 and9) and used to estimate the adsorption parameters listed in Table 6. According to R^2 and SD values, the BPA and diuron experimental data fitted better with Langmuir model for all theprepared CMs. According to the assumptions of the Langmuir model, it is demonstrated that (i) BPA and diuron are chemically adsorbed on a fixed number of distinct sites on the CMsurface, each site holding at most one BPA or diuron species;
(ii) all sites on CM surface are energetically equal; and (iii)there are no interactions between adsorbate molecules on adjacent sites. Based on Table 6, the maximum monolayer ad- sorption capacities (Q_{max}) for BPA are following the order: CM11-700 (476 mg g^{-1}) > CM14-600 (454 mg g^{-1})> CM14- 700 (434 mg g^{-1}) > CM11-600 (384 mg g^{-1}). Concerning diuron, the Q_{max} order is as follows: CM11-700 (434 mg g^{-1}) > CM14-600 (344 mg g^{-1}) > CM14-700 (322 mg g^{-1})> CM11-600 (312 mg g^{-1}). The adsorption order of CMs forBPA and diuron was the same as that of specific surface area. A CM with a higher S_{BET} is expected to have a higher uptakecapacity of pollutants in aqueous media.

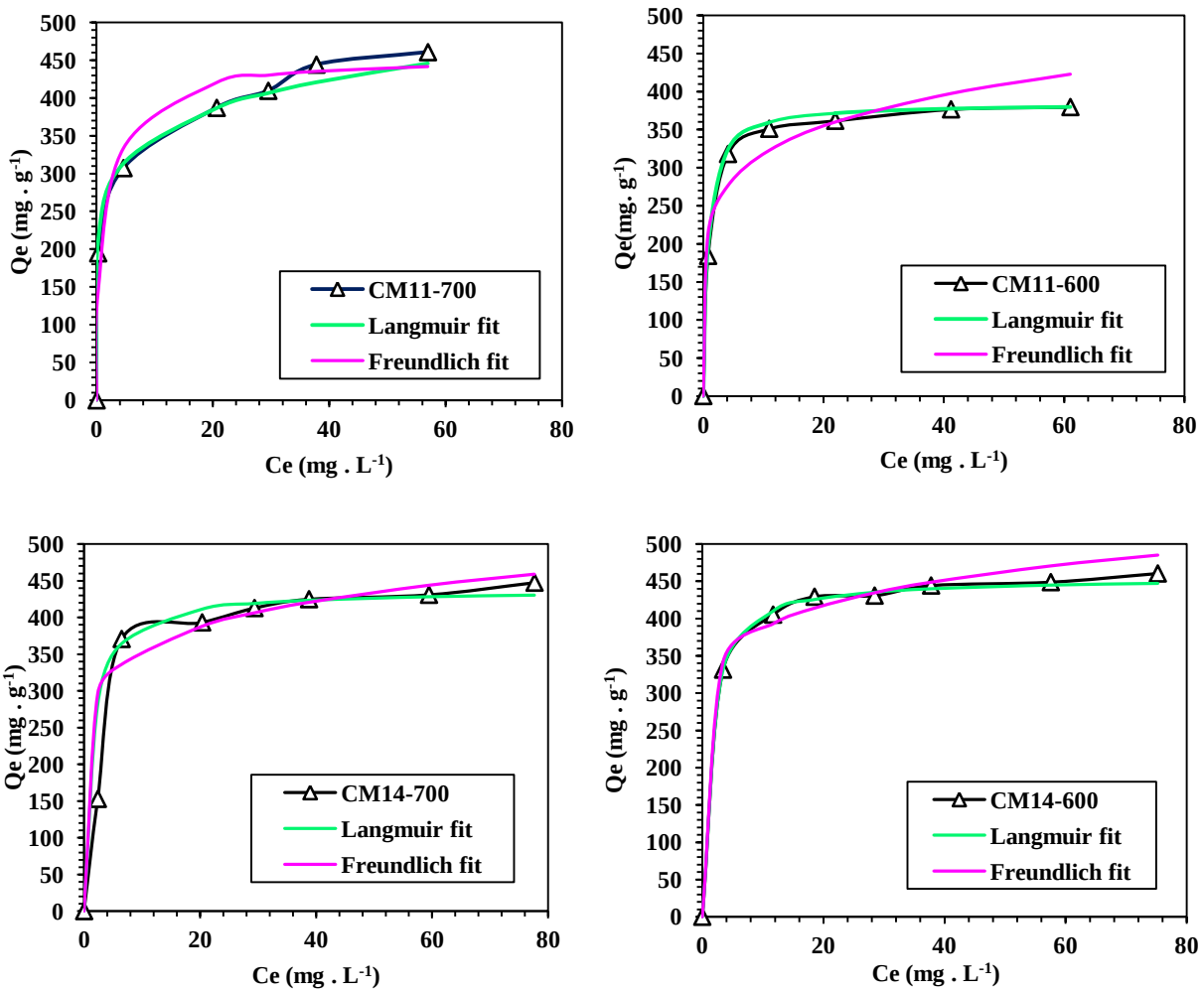

Fig 8. Nonlinear isotherm models: Langmuir and Freundlich for BPA adsorption

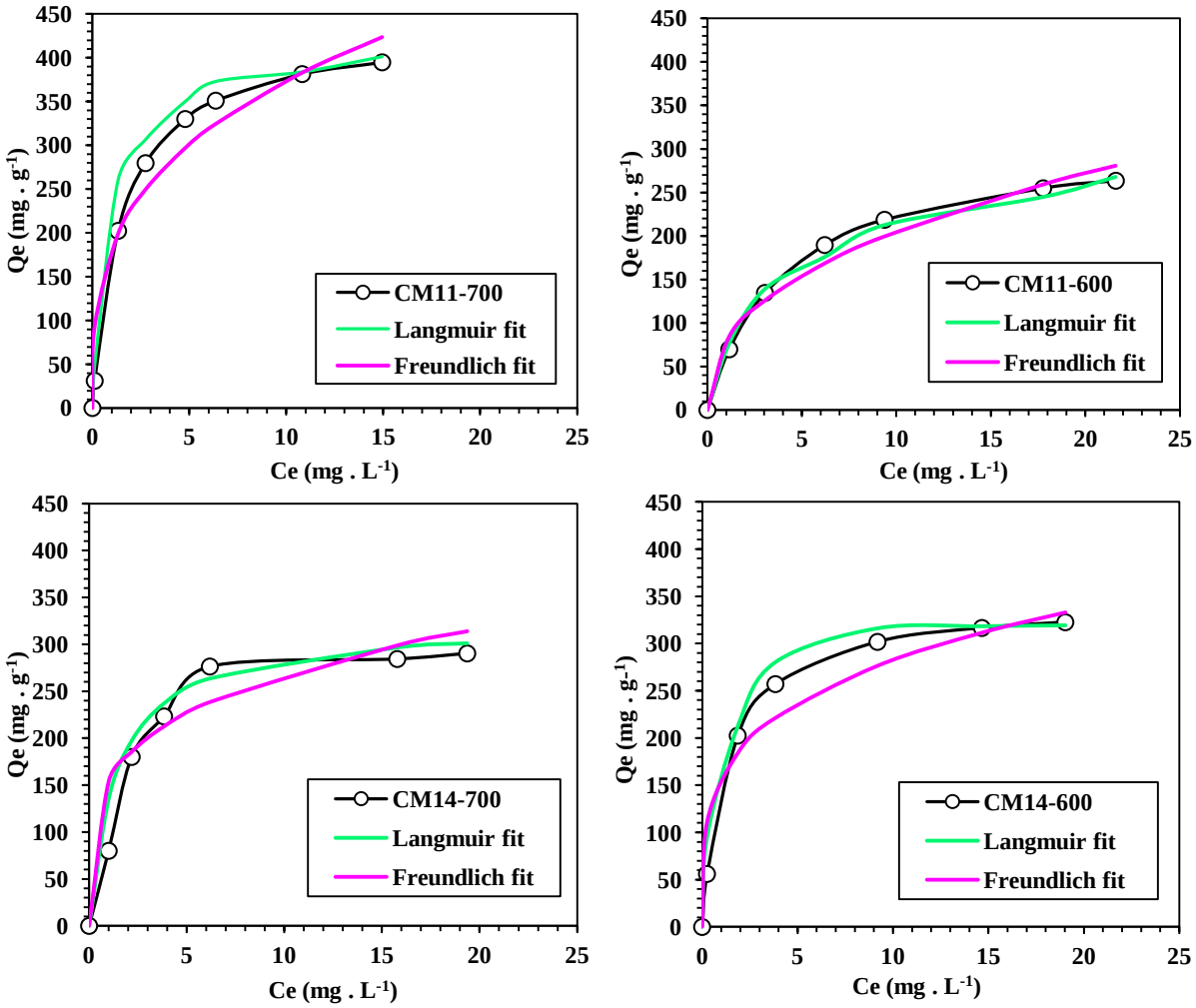

Fig 9. Nonlinear isotherm models: Langmuir and Freundlich for Diuron adsorption

Table 6. Isotherm model parameters for the adsorption of BPA and Diuron.

	Bisphenol A			
	CM11-700	**CM14-600**	**CM14-700**	**CM11-600**
Langmuir				
Qmax (mg . g^{-1})	476	454	434	384
K_L (L . mg^{-1})	0.4	1.3	1.6	1.3
R^2	0.994	0.998	0.996	0.999
SD (mg . g^{-1})	18	5	13	6
Freundlich				
K_F (mg . g^{-1}) (L . mg^{-1})$^{1/n}$	253	297	226	201
n	7.1	8.8	6.1	5.3
R^2	0.910	0.931	0.974	0.985
SD (mg . g^{-1})	36	13	18	17
	Diuron			
	CM11-700	**CM14-600**	**CM14-700**	**CM11-600**
Langmuir				
Qmax (mg . g^{-1})	434	344	322	312
K_L (L . mg^{-1})	0.6	0.3	0.7	0.2
R^2	0.986	0.991	0.989	0.994
SD (mg . g^{-1})	14	14	13	6
Freundlich				
K_F (mg . g^{-1}) (L . mg^{-1})$^{1/n}$	182	156	153	79
n	3.2	3.9	4.1	2.4
R^2	0.973	0.968	0.948	0.970
SD (mg . g^{-1})	40	22	30	11

3.5. Temperature effect on the adsorption and thermodynamics study

To study the BPA and diuron adsorption onto CMs in more details, the experiments were performed at different temperatures (20, 40, and 60 °C). The BPA and diuron concentrations used in the experiments were 20 mg L^{-1} and 35 mg L^{-1}, respectively. The results presented in Fig. 10 shows that the adsorption capacity decreases by increasing the temperature for all the CMs. For example, the adsorption capacity for BPA on CM11-700 was 334 mg g^{-1} at 20 °C and decreased to 221 mg g^{-1} at 60 °C, whereas for diuron at 20 °C, the adsorption capacity was 420 mg g^{-1} and at 60 °C it was diminished to 185 mg g^{-1}. Therefore, the adsorption of BPA and diuron onto CMs is exothermic in nature (Deng et al. 2012; Kwon and Lee 2015).

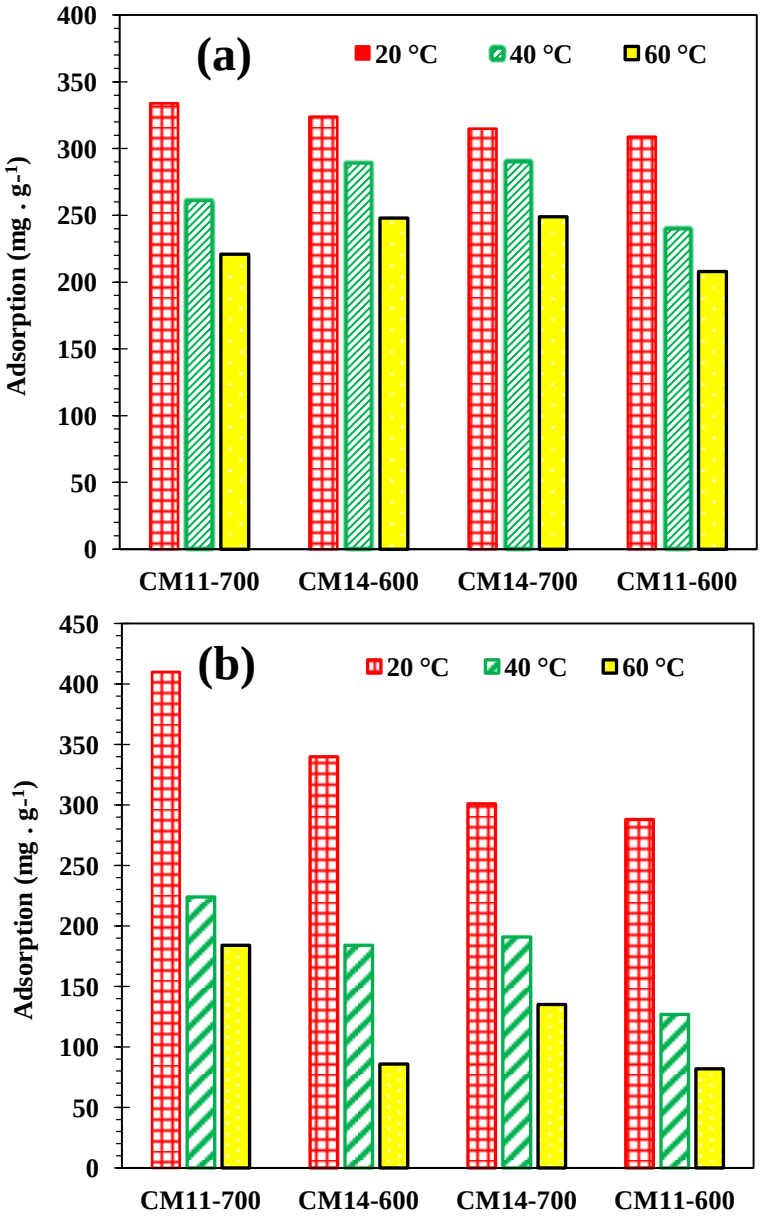

Fig 10. Effect of temperature on BPA (a) and Diuron (b) adsorption onto CMs.

The nature of adsorption can be confirmed and the adsorption mechanism (i.e., physical or chemical) can be reasonably determined through the examination of adsorption thermodynamics. The thermodynamic parameters ($\Delta G°$, $\Delta H°$, and $\Delta S°$) of BPA and diuron removal by CMs can be assessed by the van't Hoff approach and Gibbs free energy equations presented in Table 2 (Anastopoulos and Kyzas 2016; Tran et al. 2017). Table 7 lists the thermodynamic parameters calculated using Fig. 11. The negative $\Delta G°$ values of BPA and diuron adsorption onto CMs at all examined temperatures point out that the BPA and diuron adsorption phenomenon occurred spontaneously. Moreover, the negative ($\Delta S°$) value reveals that the organization of BPA and diuron molecules at the solid/solution interface during the adsorption process on CMs becomes less random when the temperature increases. The negative value of $\Delta H°$ indicates that the BPA and diuron adsorption is exothermic in nature. An exothermic process is obviously attributed to physical adsorption (physisorption) with weak adsorption force (i.e., van der Waals interaction type) (Van et al. 2019) Therefore, BPA and diuron adsorbed on CMs tend to desorb when temperature increases.

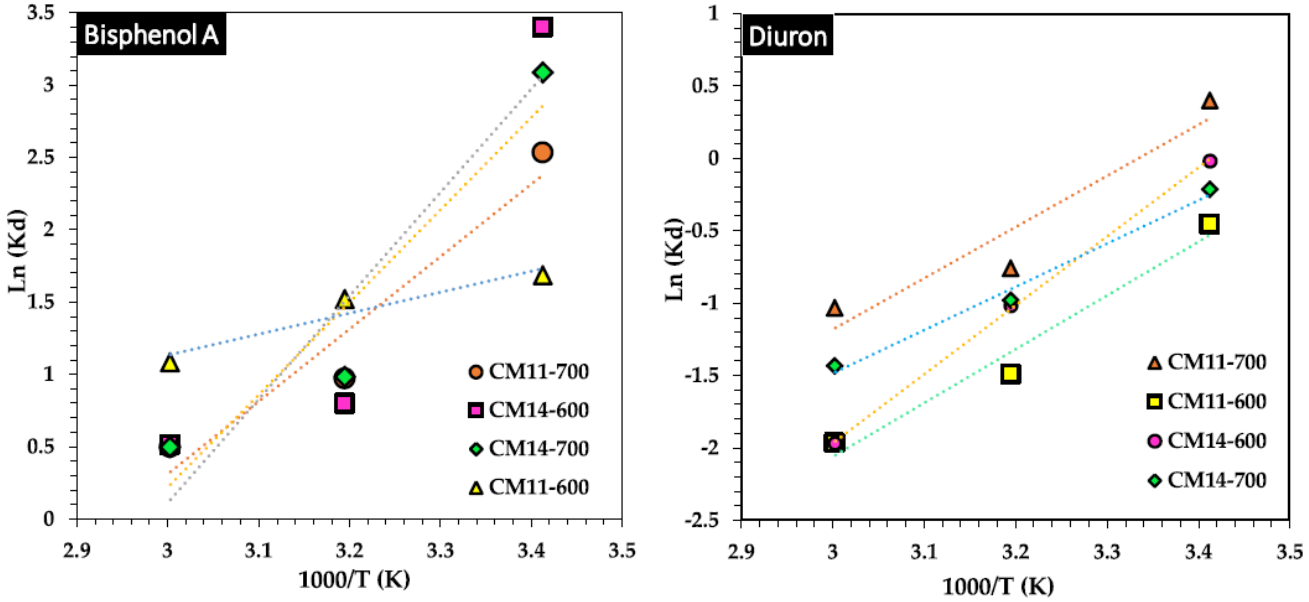

Fig 11. The plot of Ln (K_d) versus 1/T for thermodynamic parameters for the adsorption of Bisphenol A and Diuron

Table 7. Thermodynamic parameters for the adsorption of BPA and Diuron

	Adsorbents	ΔH^0 (kJ . mol^{-1})	ΔS^0 (J . mol^{-1} . K^{-1})	ΔG^0 (kJ . mol^{-1})		
				293 K	313 K	333 K
BPA	CM11-700	-59.40	-177.40	-8.30	-2.10	-1.40
	CM14-600	-41.60	-122.30	-6.20	-2.50	-1.40
	CM14-700	-53.10	-157.60	-7.50	-2.50	-1.40
	CM11-600	-32.90	-99.30	-4.10	-3.90	-3.00
Diuron	CM11-700	-29.30	-97.90	-0.90	-1.90	-2.80
	CM14-600	-39.50	-134.80	-0.04	-2.60	-5.40
	CM14-700	-24.80	-86.80	-0.50	-2.50	-3.90
	CM11-600	-30.90	-109.50	-1.10	-3.90	-5.40

The comparison of the BPA and diuron adsorption capacity on several adsorbents reported in the literature, and including our results, is presented in Table 8. Those results evidenced that the materials prepared in the present study exhibited one of the highest adsorption capacities and specific surface area.

Table 8. Ad**sorption capacities of BPA and Diuron on CMs compared to the literature.**

Adsorbent	Raw material	Preparation parameters	Specific surface area ($m^2 . g^{-1}$)	Adsorption capacity ($mg . g^{-1}$)	Reference
Bisphenol A					
CM11-700	**Olive kernels**	**CA:H_3PO_4 TA: 700 °C**	**1472**	**464**	**Current study**
Activated carbon	Wood ship	**TA**: 800 °C	1119	23	(Nakanishi et al. 2002)
Graphene	Graphene oxide	**Hummers method**	327	181	(Xu and Zhu 2012)
Mesoporous carbon (CMK3)	Tri-block copolymer P123	**CA**: HCl solution **TA**:500 °C	920	296	(Sui et al. 2011)
Activated carbon	Commercial activated carbon	**CA:** HNO_3 **TA:** 600 °C	1760	432	(Liu et al. 2009)
Activated carbon	Olive-mill waste	**CA:** KOH **TA:** 500 °C	1225	397	(Bautista-Toledo et al., 2014)
Activated carbon	Scrap tyre	**CA:** KOH **TA:** 750 °C	700	123	(Acosta et al. 2018b)
Biochar	Alfalfa (Medicago sativa L.) (grown crops)	**TA:** 650 °C	405	90	(Choi and Kan, 2019)
Activated carbon	Asphalt	**CA:** KOH **TA:** 400 °C	813	271	(Javed et al. 2018)
Diuron					
CM11-700	**Olive kernels**	**CA:** H_3PO_4 **TA:** 700 °C	**1472**	**458**	**Current study**
Activated carbon	Commercial activated carbon	ND	2128	293	(López-Ramón et al. 2007)
Activated carbon	Granular activated carbon (GAC)	Demineralized by HF and HCl	776	279	(Fontecha-Cámara et al. 2006)
Activated carbon	Grape seeds	**CA:** H_2SO_4 & H_3PO_4 **TA:** 500 °C	1139	38	(Bahri et al. 2012)
Carbon Nanotubes (CNT)	Commercial CNT	ND	258	39	(Sun et al. 2012)

Activated carbon	Grape seeds	**CA:** H_3PO_4 **TA:** 500 °C	1139	15	(Al Bahri et al. 2012)
Bottom ash	Bottom ash waste	**TA:** 200 °C	ND	360	(Zbair et al. 2020)
Activated carbon	Wood composites	**PA**:CO_2 **TA**: 800 °C	1211	435	(Cansado et al. 2017)
Activated carbon	Baobab wood	**PA:** CO_2 **TA:** 900 °C	2130	400	(Tchikuala et al. 2017)

***TA:** Thermal activation.
***CA:** Chemical activation.
***PA:** Physical activation.
***ND**: Not defined.

Conclusion

In this paper, we reported successful preparation of porous carbon materials (CMs) derived from olive kernels waste. During the preparation, we investigated the effect of pyrolysis temperature and mass ratio of H_3PO_4. The use of phosphoric acid as activating agent with the mass ratio (raw material: activating agent) equal to (1:1) followed by a pyrolysis at 700 °C results in the highest specific surface area (1472 $m^2\ g^{-1}$) and excellent adsorption performance of the CM. The adsorption capacities according to Langmuir model reached 476 mg g^{-1} and 434 mg g^{-1} for BPA and diuron, respectively, which are superior to the ones reported for most of the carbon adsorbents. The kinetics of BPA and diuron adsorption onto the CMs fitted well with the pseudo-second order model. Moreover, the ad- sorption process of BPA and diuron onto CMs was spontaneous ($\Delta G° < 0$) and exothermic ($\Delta H° < 0$) involving physical adsorption. This work evidenced that transformation of agricultural biomass waste can lead to an economic and effective adsorbent for the removal of organic pollutants from water.

Conflicts of interest

Authors declare no conflict of interest.

Acknowledgments

This work has received funding from Erasmus+ Global program between University of Oulu, Finland and University of Chouaïb Doukkali, Morocco (2017-2019).

The authors express their gratitude to the PHC-Maghreb project (16-MAG 11) for the financial support. The authors acknowledge financial support from the European Union (ERDF) and "Région Nouvelle Aquitaine".

References

Acosta R, Nabarlatz D, Sánchez-Sánchez A, Jagiello J, Gadonneix P, Celzard A (2018) Adsorption of bisphenol A on KOH-activated tyre pyrolysis char. J Environ Chem Eng: Elsevier 6(1):823-833. https://doi.org/10.1016/J.JECE.2018.01.002

Al Bahri M, Calvo L, Gilarranz MA, Rodriguez JJ (2012a) Activated carbon from grape seeds upon chemical activation with phosphoric acid: application to the adsorption of diuron from water. Chem Eng J348:356-356. https://doi.org/10.1016/j.cej.2012.07.053

Al Bahri M, Calvo L, Lemus J, Gilarranz MA, Palomar J, Rodriguez JJ (2012b) Mechanistic understanding of the behavior of diuron in the adsorption from water onto activated carbon. Chem Eng J: Elsevier 198:199-346:354. https://doi.org/10.1016/j.cej.2012.06.011

Alslaibi TM, Ismail A, Mohd AA, Ahmed AF (2013) Cadmium removal from aqueous solution using microwaved olive stone activated car- bon. Biochem Pharmacol 589:599-599. https://doi.org/10.1016/j.jece.2013.06.028

Anastopoulos I, Kyzas GZ (2016) Are the thermodynamic parameters correctly estimated in liquid-phase adsorption phenomena? J Mol Liq 174:185-185. https://doi.org/10.1016/j.molliq.2016.02.059

Bahri MA, Calvo L, Lemus J, Gilarranz MA, Palomar J, Rodriguez JJ (2012) Mechanistic understanding of the behavior of diuron in the adsorption from water onto activated carbon. Chem Eng J:Elsevier 198:199-346:354. https://doi.org/10.1016/j.cej.2012.06.011

Bautista-Toledo I, Ferro-García MA, Rivera-Utrilla J, Moreno-Castilla C, Fernández FJV (2005) Bisphenol A removal from water by activated carbon. Effects of carbon characteristics and solution chemistry. Environ Sci Technol: American Chemical Society 6246:6250. https://doi.org/10.1021/es0481169

Bautista-Toledo I, Rivera-Utrilla J, Ocampo-Pérez R, Carrasco-Marín F, Sánchez-Polo M (2014) Cooperative adsorption of bisphenol A and chromium(III) ions from water on activated carbons prepared from olive-mill waste. Carbon:Elsevier 338:350-350. https://doi.org/10.1016/j.carbon.2014.02.073

Bhatnagar A. and Anastopoulos I. (2017) "Adsorptive removal of bisphenol A (BPA) from aqueous solution: A review," Chemosphere 168. https://doi.org/10.1016/j.chemosphere.2016.10.121

Bolivar JM, Gascon V, Marquez-Alvarez C, Blanco RM, Nidetzky B (2017) Oriented coimmobilization of oxidase and catalase on tailor-made ordered mesoporous silica. Langmuir 5065:5076- 5076. https://doi.org/10.1021/acs.langmuir.7b00441

Boshir Ahmed M, Hasan Johir MA, Zhou JL, Hao Ngo H, Duc Nghiem L, Richardson C, Ali Moni M, Bryant MR (2019) Activated carbon preparation from biomass feedstock: clean production and carbon dioxide adsorption. J Clean Prod 225:405-413. https://doi.org/10.1016/j.jclepro.2019.03.342

Cansado IPP, Mourão PAM, Gomes JAFL, Almodôvar V (2017) Adsorption of MCPA, 2,4-D and diuron onto activated carbons from wood composites. Ciencia e Tecnologia dos Materiais Elsevier 224: 228. https://doi.org/10.1016/j.ctmat.2016.07.005

Choi YK, Kan E (2019) Effects of pyrolysis temperature on the physicochemical properties of alfalfa-derived biochar for the adsorption of bisphenol A and sulfamethoxazole in water. Chemosphere: Elsevier Ltd 741:748-748. https://doi.org/10.1016/j.chemosphere.2018.11.151

Deng J, Shao Y, Gao N (2012) Multiwalled carbon nanotubes as adsor bents for removal of herbicide diuron

from aqueous solution. Chem Eng J 193-194:339-347. https://doi.org/10.1016/j.cej.2012.04.051

Desbiolles A (2016) Perturbateurs endocriniens, Revue Francophone d'Orthoptie. https://www.e-cancer.fr/Comprendre-prevenir-depister/Reduire-les-risques-de-cancer/Environnement/Les-perturbateurs-endocriniens. Accessed Dec 2019

Dizbay-Onat M, Vaidya UK, Lungu CT (2017) Preparation of industrial sisal fiber waste derived activated carbon by chemical activation and effects of carbonization parameters on surface characteristics. Ind Crop Prod 583:590-590. https://doi.org/10.1016/j.indcrop.2016. 11.016

Fontecha-Cámara MÁ, López-Ramón MV, Álvarez-Merino MA, Moreno-Castilla C (2006) Temperature dependence of herbicide adsorption from aqueous solutions on activated carbon fiber and cloth. Langmuir: American Chemical Society 9586:9590-9590. https://doi.org/10.1021/la061666v

Fontecha-Cámara MA, López-Ramón MV, Álvarez-Merino MA, Moreno-Castilla C (2007) Effect of surface chemistry, solution pH, and ionic strength on the removal of herbicides diuron and amitrole from water by an activated carbon fiber. Langmuir: American Chemical Society 1242:1247-1247. https://doi.org/10. 1021/la062200f

Fontecha-Cámara MA, López-Ramón MV, Pastrana-Martınez LM, Moreno-Castilla C (2008) Kinetics of diuron and amitrole adsorp tion from aqueous solution on activated carbons. J Hazard Mater 472:477-477. https://doi.org/10.1016/j.jhazmat.2007.12.043

Freundlich H (1907) Über die Adsorption in Lösungen. Z Phys Chem 57U(1). https://doi.org/10.1515/zpch-1907-5723 (in German)

Fu W, Zhang W (2018) Microwave-enhanced membrane filtration for water treatment. J Membr Sci 97:104-104. https://doi.org/10.1016/j.memsci.2018.09.064

García G, Calero de Hoces M, Martinez Garcia C (2014) Characterization and modeling of pyrolysis of the two-phase olive mill solid waste. Fuel Process Technol:104-111. https://doi.org/10.1016/j.fuproc.2014.04.020

Garg VK, Gupta R, Yadav AB, Kumar R (2003) Dye removal from aqueous solution by adsorption on treated sawdust. Bioresour Technol 121:124-124. https://doi.org/10.1016/S0960-8524(03)00058-0

Giacomazzi S, Cochet N (2004) Environmental impact of diuron trans- formation: a review. Chemosphere 1021:1032-1032. https://doi. org/10.1016/j.chemosphere.2004.04.061

Hazzaa R, Hussein M (2015) Adsorption of cationic dye from aqueous solution onto activated carbon prepared from olive stones. Environ Technol Innov 36:51-51. https://doi.org/10.1016/j.eti.2015.04.002

Ho YS, McKay G (1999) Pseudo-second order model for sorption processes. Process Biochem 451:465-465. https://doi.org/10.1016/ S0032-9592(98)00112-5

Javed H, Luong D, Lee CG, Zhang D, Tour JM, Alvarez PJJ (2018) Efficient removal of bisphenol-A by ultra-high surface area porous activated carbon derived from asphalt. Carbon: Elsevier Ltd 441: 448-448. https://doi.org/10.1016/j.carbon.2018.08.038

Jiang Y, Xie Q, Zhang Y, Geng C, Yu B, Chi J (2019) Preparation of magnetically separable mesoporous activated carbons from brown coal with Fe_3O_4. Int J Min Sci Technol 513:519-519. https://doi. org/10.1016/j.ijmst.2019.01.002

Kiliç M, Apaydin-Varol E, Pütün AE (2012) Preparation and surface characterization of activated carbons from Euphorbia rigida by chemical activation with $ZnCl_2$, K_2CO_3, NaOH and H_3PO_4. Appl Surf Sci: Elsevier 247:254. https://doi.org/10.1016/j.apsusc.2012. 07.155

Kumar A, Jena HM (2016) Preparation and characterization of high sur- face area activated carbon from Fox nut (Euryale ferox) shell by chemical activation with H_3PO_4. Results Phys: Elsevier 651:658-

658. https://doi.org/10.1016/J.RINP.2016.09.012

Kwon J, Lee B (2015) Bisphenol A adsorption using reduced graphene oxide prepared by physical and chemical reduction methods. Chem Eng Res Des 519:529-529. https://doi.org/10.1016/j.cherd.2015.09.007

Langmuir I (1916) The constitution and fundamental properties of solids and liquids. Part I. Solids. J Am Chem Soc 2221:2295-2295. https://doi.org/10.1021/ja02268a002

Lee HM, An KH, Chung DC, Jung SC, Park YK, Park SJ (2019) Comparison studies on pore development mechanisms of activated hard carbons from polymeric resins and their applications for electrode materials. Renew Energy 116:122-122. https://doi.org/10. 1016/j.renene.2018.11.020

Liu G, Ma J, Li X, Qin Q (2009) Adsorption of bisphenol A from aqueous solution onto activated carbons with different modification treatments. J Hazard Mater 1275:1280-1280. https://doi.org/10.1016/j.jhazmat.2008.09.038

Liu J, Morales-Narváez E, Vicent T, Merkoçi A, Zhong GH (2018) Microorganism-decorated nanocellulose for efficient Diuron removal. Chem Eng J: Elsevier 1083:1091-1091. https://doi.org/10.1016/j.cej.2018.08.035

López-Ramón MV, Fontecha-Cámara M, Álvarez-Merino M, Moreno- Castilla C (2007) Removal of diuron and amitrole from water under static and dynamic conditions using activated carbons in form of fibers, cloth, and grains. Water Res 2865:2870-2870. https://doi.org/10.1016/j.watres.2007.02.059

López-Ramón MV, Ocampo-Pérez R, Bautista-Toledo MI, Rivera- Utrilla J, Moreno-Castilla C, Sánchez-Polo ML (2019) Removal of bisphenols A and S by adsorption on activated carbon clothes enhanced by the presence of bacteria. Sci Total Environ 767:776-776. https://doi.org/10.1016/j.scitotenv.2019.03.125

Lorenzo M, An Campo J, Pic Y (2018) Analytical challenges to deter- mine emerging persistent organic pollutants in aquatic ecosystems. Trends Anal Chem 137:155-155. https://doi.org/10.1016/j.trac.2018.04.003

Michałowicz J (2014) Bisphenol A - sources, toxicity and biotransfor mation. Environ Toxicol Pharmacol 738:758. https://doi.org/10. 1016/j.etap.2014.02.003

Nakanishi A, Tamai M, Nakamura T (2002) Adsorption characteristics of bisphenol A onto carbonaceous materials produced from wood chips as organic waste. J Colloid Interface Sci 409:418-418. https://doi.org/10.1006/jcis.2002.8471

Nathan AJ, Scobell A (2012) How China sees America. Foreign Affairs 1:39. https://doi.org/10.1017/CBO9781107415324.004

Nieto-Delgado C, Rangel-Mendez JR (2011) Production of activated car- bon from organic by-products from the alcoholic beverage industry: surface area and hardness optimization by using the response surface methodology. Ind Crop Prod 1528:1537-1537. https://doi.org/10.1016/j.indcrop.2011.05.014

Özveren U, Özdoğan ZS (2013) Investigation of the slow pyrolysis kinetics of olive oil pomace using thermo-gravimetric analysis coupled with mass spectrometry. Biomass Bioenergy 168:179- 179. https://doi.org/10.1016/j.biombioe.2013.08.011

Rice D, Paul W, François P, Sergi GS (2018) Electrochemical self- cleaning anodic surfaces for biofouling control during water treat- ment. Electrochem Commun 83:87-87. https://doi.org/10.1016/j.elecom.2018.10.002

Som MP, Lemée L, Amblès A (2009) Stability and maturity of a green waste and biowaste compost assessed

on the basis of a molecular study using spectroscopy, thermal analysis, thermodesorption and thermochemolysis. Bioresour Technol 4404:4416. https://doi.org/10.1016/j.biortech.2009.04.019

Sui Q, Huang J, Liu Y, Chang X, Ji G, Deng S (2011) Rapid removal of bisphenol A on highly ordered mesoporous carbon. J Environ Sci 177:182. https://doi.org/10.1016/S1001-0742(10)60391-9

Sun K, Zhang Z, Gao B, Wang Z, Xu D, Jin J (2012) Adsorption of diuron, fluridone and norflurazon on single-walled and multi- walled carbon nanotubes. Sci Total Environ 1:7. https://doi.org/10.1016/j.scitotenv.2012.08.022

Supong A, Bhomick P, Baruah M, Pongener C, Sinha U, Sinha D (2019) Adsorptive removal of bisphenol A by biomass activated carbon and insights into the adsorption mechanism through density functional theory calculations. Sustain Chem Pharm: Elsevier 13:100159. https://doi.org/10.1016/j.scp.2019.100159

Tchikuala E, Mourão P, Nabais J (2017) Valorisation of natural fibres from African Baobab wastes by the production of activated carbons for adsorption of diuron. Procedia Eng: Elsevier Ltd 399:407. https://doi.org/10.1016/j.proeng.2017.07.056

Thommes M, Kaneko K, Neimark AV, Olivier JP, Rodriguez-Reinoso F, Rouquerol J (2015) Physisorption of gases, with special reference to the evaluation of surface area and pore size distribution (IUPAC Technical Report). Pure Appl Chem 1051:1069. https://doi.org/10.1515/pac-2014-1117

Tolosana-Moranchel A, Ovejero D, Barco B, Bahamonde A, Díaz E, Faraldos M (2019) An approach on the comparative behavior of chloro/nitro substituted phenols photocatalytic degradation in water. J Environ Chem Eng 1:26. https://doi.org/10.1016/j.jece.2019. 103051

Tran HN, You SJ, Hosseini-Bandegharaei A, Chao HP (2017) Mistakes and inconsistencies regarding adsorption of contaminants from aqueous solutions: a critical review. Water Res 88:116. https://doi.org/10.1016/j.watres.2017.04.014

Tran HN, Chao HP, You SJ (2018) Activated carbons from golden shower upon different chemical activation methods: synthesis and characterizations. Adsorpt Sci Technol SAGE Publications Ltd STM 95: 113-113. https://doi.org/10.1177/0263617416684837

Tsai WT, Chang CY (1995) Surface characterization and thermodynamics of adsorption of methylene chloride on activated carbons. J Environ Sci Health A :Taylor & Francis 525:535. https://doi.org/10.1080/10934529509376215

Tsai WT, Lai CW, Su TY (2006) Adsorption of Bisphenol-A from aqueous solution onto minerals and carbon adsorbents. J Hazard Mater 169:75-175. https://doi.org/10.1016/j.jhazmat.2005.10.055

Van HT, Nguyen LH, Nguyen VD, Nguyen XH, Nguyen TH, Nguyen TV, Vigneswaran S, Rinklebe J, Tran HN (2019) Characteristics and mechanisms of cadmium adsorption onto biogenic aragonite shells-derived biosorbent: Batch and column studies. J Environ Manag 535:548-548. https://doi.org/10.1016/j.jenvman.2018.09.079

Wang J, Huang C, Allen H, Cha DK, Kim DW (1998) Adsorption characteristics of dye onto sludge particulates. J Colloid Interface Sci 518:528-528. https://doi.org/10.1006/jcis.1998.5875

Wang S, Nam H, Nam H (2020) Preparation of activated carbon from peanut shell with KOH activation and its application for H_2S ad- sorption in confined space. J Environ Chem Eng: Elsevier BV 8: 103683. https://doi.org/10.1016/j.jece.2020.103683

Xing X, Jiang W, Li S, Zhang X, Wang W (2019) Preparation and analysis of straw activated carbon synergetic catalyzed by $ZnCl_2$ -H_3PO_4 through hydrothermal carbonization combined with ultrasonic assisted immersion pyrolysis. Waste Manag 64:72-72. https://doi.org/10.1016/j.wasman.2019.04.002

Xu J, Wang L, Zhu Y (2012) Decontamination of bisphenol A from aqueous solution by graphene adsorption. Langmuir:American Chemical Society 8418:8425-8425. https://doi.org/10.1021/la301476p

Yang K, Wu W, Jing Q, Zhu L (2008) Aqueous adsorption of aniline, phenol, and their substitutes by multi-walled carbon nanotubes. Environ Sci Technol: American Chemical Society 42(21):7931-7936. https://doi.org/10.1021/es801463v

Yorgun S, Yıldız D (2015) Preparation and characterization of activated

carbons from Paulownia wood by chemical activation with H_3PO_4.J Taiwan Inst Chem Eng 122:131-131. https://doi.org/10.1016/j.jtice.2015.02.032

Zbair M, Anfar Z, Ait Ahsaine H, El Alem N, Ezahri M (2018a) Acridine orange adsorption by zinc oxide/almond shell activated carbon composite: operational factors, mechanism and performance optimization using central composite design and surface modeling. J Environ Manag 383:397-397. https://doi.org/10.1016/j.jenvman.2017.10.058

Zbair M, Ainassaari K, El Assal Z, Ojala S, El Ouahedy N, Keiski RL (2018b) Steam activation of waste biomass: highly microporous carbon, optimization of bisphenol A, and diuron adsorption by response surface methodology. Environ Sci Pollut Res 25:35657- 35671. https://doi.org/10.1007/s11356-018-3455-3

Zbair M, Ainassaari K, Drif A (2018c) Toward new benchmark adsorbents: preparation and characterization of activated carbon from argan nut shell for bisphenol A removal. Environ Sci Pollut Res 1869:1882-1882. https://doi.org/10.1007/s11356-017-0634-6

Zbair M, Bottlinger M, Ainassaari K, Ojala S, Stein O, Keiski RL (2018d) Hydrothermal carbonization of argan nut shell: functional mesoporous carbon with excellent performance in the adsorption of bisphenol A and diuron. Waste Biomass Valoriz : Springer Netherlands 11:1565-1584. https://doi.org/10.1007/s12649-018-00554-0

Zbair M, Hadrami A, El Bellarbi A, Monkade M, Zradba A, Brahmi R (2020) Herbicide diuron removal from aqueous solution by bottom ash: kinetics, isotherm, and thermodynamic adsorption studies. J Environ Chem Eng 8:103667. https://doi.org/10.1016/j.jece.2020.103667